Design of a Flutter Mode Controller Using Positive Real Feedback

Marc Takahashi* and G.L. Slater†
University of Cincinnati, Cincinnati, Ohio

The use of positive real feedback for the design of a flutter mode control system is examined. Results indicate that this technique is a meaningful synthesis procedure for the design of low-order controllers. The synthesis is achieved through the design of a positive real observer using a low-order approximation to the governing system equations. Results obtained for a realistic aeroelastic model show that flutter dynamic pressure can be increased by more than 50%. The effect of unmodeled phase shift caused by aerodynamic and actuation lags can be avoided in the positive real design by suitable choice of control bandwidth. This technique thus appears as a viable design technique for flutter and aeroelastic modal control.

Nomenclature

A_i, B_i	= unsteady aerodynamic coefficient matrices
b	= wing semichord (reference length)
F, G, H	= state space matrices
F_{CL}	= nominal closed-loop matrix
q_d	= dynamic pressure
q	= scalar weight in Lyapunov equation ($Q = qI$)
Q	= positive definite matrix in Lyapunov equation
Q_A	= matrix of aerodynamic forces
Q_D, R_D	= matrices in linear optimal control performance index
P	= positive definite solution of Lyapunov equation
v	= wing velocity
x_1	= mode displacement
x_2	= mode velocity state
x_3, x_4	= aerodynamic lag states
x_5	= actuator states
β_i	= aerodynamic lag term
δ_c	= commanded control surface deflection

Subscripts

A	= actuator
m	= model
r	= residual

Introduction

ACTIVE control of aircraft flutter modes is an important and active area of current control research. The flutter problem is similar to the large space structure problem in that there are numerous (theoretically infinite) flexible modes affecting the motion. The problem is complicated by the interaction of the aerodynamics with the elastic structure, which may change the frequency and damping characteristics of the modes and also will introduce additional nonrational dynamic terms into the governing equations. This paper deals with problems of defining an adequate model, formulating a control law, and ensuring the robustness of the controller. The approach used in this paper is the concept of hyperstability or positivity of transfer functions suggested in Ref. 1. This paper presents the application of positivity methodology applied to a realistic wing flutter problem.

Submitted Aug. 6, 1984; presented as Paper 84-1869 at the AIAA Guidance and Control Conference, Seattle, WA, Aug. 20-22, 1984; revision received Sept. 6, 1985.

*Graduate Student, Department of Aerospace Engineering and Engineering Mechanics. Student Member AIAA.

†Professor, Department of Aerospace Engineering and Engineering Mechanics. Member AIAA.

Theory

To see how positivity concepts can be used, the following theorems and definitions are presented.[2-4]

Theorem 1. Given the square transfer matrices $G(s)$ and $H(s)$, the system of Fig. 1 is asymptotically stable if at least one of the transfer matrices is positive real and the other is strictly positive real.

If the feedforward and the feedback blocks are single-input/single-output systems, the square transfer matrices become transfer functions $G(s)$ and $H(s)$, and the following definitions apply.

Definition 1. A rational function $G(s)$ of the complex variables $s = \sigma + j\omega$ is *positive real* if:

1) $G(s)$ is real for real s.

2) $G(s)$ has no poles in the open right half-plane, $Re(s) > 0$.

3) The eventual poles of $G(s)$ on the real axis $Re(s) = 0$ are distinct and the associated residues are real and positive or null.

4) For all real ω for which $s = j\omega$ is not a pole of $G(s)$, $Re(G(j\omega)) \geq 0$.

Definition 2. A rational function $G(s)$ of the complex variables $s = \sigma + j\omega$ is *strictly positive real* if:

1) $G(s)$ is real for real s.

2) $G(s)$ has no poles in the closed right half-plane $Re(s) \geq 0$

3) For all real ω, $Re(G(j\omega)) > 0$.

In the frequency domain, Definitions 1 and 2 imply that there is no more than 90-deg phase shift in either lead or lag. Definition 2 requires that the phase shift be strictly less than 90 deg. Theorem 1, when applied to single-input/single-output systems, simply imposes a restriction on the total amount of phase shift that the $G(s)H(s)$ transfer function may have. Since $G(s)H(s)$ will not have more than 180-deg lead or lag, no encirclements of the -1 point will occur on the Nyquist plot, and thus instability cannot occur in the feedback system. An alternate criteria, more applicable for state space models, can be found in the following theorem:[2]

Theorem 2. For the system described in stable variable form, $\dot{X} = FX + GU$, $Y = HX$, the transfer matrix $G(s) = H[sI - F]^{-1}G$ is positive real if, and only if, a symmetric positive definite matrix P and a symmetric positive semidefinite matrix Q exists such that $PF + F^TP = -Q$, $H^T = PG$.

Design of Positive Real Feedback

The frequency response conditions for positive realness allow us to easily construct simple transfer functions, such as the first-order lag, which are positive real. For more general systems the use of Theorem 2 allows construction of feedback functions that satisfy the positivity condition. For this problem we use the modern view of the feedback element as being related to a state variable estimator. Consider a system to be controlled with input u and output y ($\dim u = \dim y = m \geq 1$). Assume, then, that a state variable approximation to the controlled system can be written as

$$\dot{x} = F_m x + G_m u, \qquad y = H_m x \tag{1}$$

A design to control this system will have the form of an estimator

$$\dot{\hat{x}} = F_m \hat{x} + G_m u + K_F(y - \hat{y}), \qquad \hat{y} = H_m \hat{x} \tag{2}$$

and a state variable feedback law of the form

$$u = -u_1 = -K\hat{x} \tag{3}$$

The feedback transfer function matrix relating output u_1 to input y is

$$H(s) = K(sI - F_T)^{-1} K_F \tag{4}$$

where $F_T = (F_m - G_m K - K_F H_m)$. If the controlled system is modeled perfectly (i.e., $F = F_m$, etc.), the closed-loop system poles are the eigenvalues of $(F_m - G_m K)$ and of $(F_m - K_F H_m)$. The matrices K and K_F can be chosen independently to satisfy optimization or pole placement criteria. If the model is not identical to the system being controlled, the true closed-loop eigenvalues may differ significantly from their design values, and stability problems may occur. In the typical flutter problem the system model is by necessity a low-order approximation to the actual infinite dimensional dynamics. Additional uncertainties are introduced due to mass variations caused by fuel, wing stores and possible structural variations. To determine a flutter controller insensitive to these uncertainties, we note that the transfer function between a control surface input and a velocity output can often be closely approximated by a positive real function. Using the methodology of Ref. 1, a positive real estimator can be chosen based on the results of Theorem 2. Using the estimator model (1-3), Theorem 2 can be written in the form

$$PF_{CL} + F_{CL}^T P = -Q + K^T H_m + H_m^T K \tag{5}$$

$$K^T = PK_F \tag{6}$$

where $F_{CL} = F_m - G_m K$.

Equations (5) and (6) can be solved for K_F, given K and Q. The choice of the Q matrix allows the design flexibility to adjust the closed-loop estimator eigenvalues.

Note that using this technique, the overall loop stability is not limited by the model validity but rather by the positive realness condition. Application of this technique to a realistic flutter problem is discussed in succeeding sections of this paper.

Flutter Model

The model used in this paper is a linear representation of the wing presented in Fig. 2. The equation of motion for the wing with the control surface is given by:[5]

$$(Ms^2 + D_s s + K_s)x_1 + q_d Q_A \begin{bmatrix} x_1 \\ x_5 \end{bmatrix} = 0 \tag{7}$$

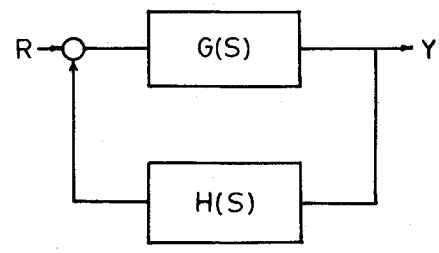

Fig. 1 Feedback structure for application of hyperstability theorem.

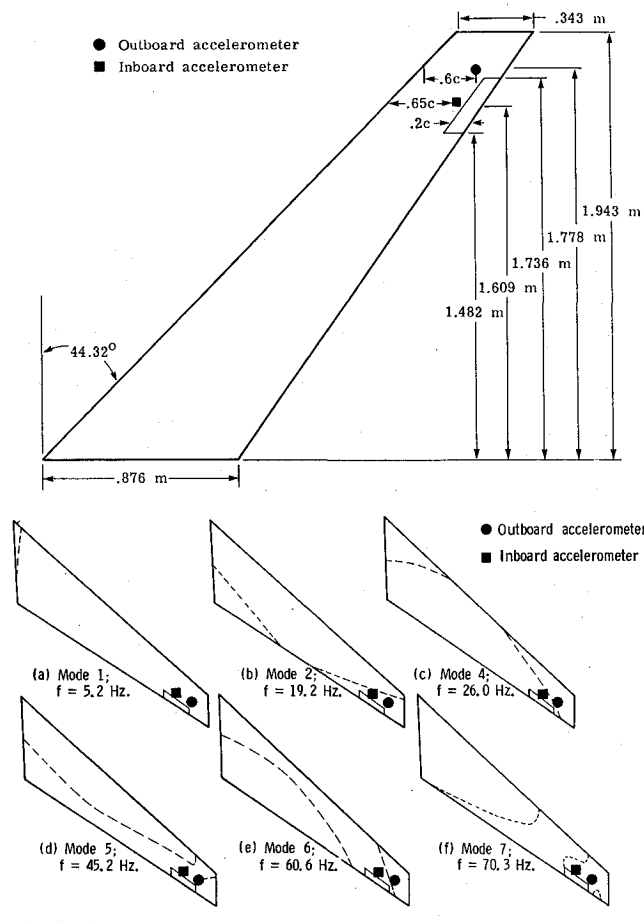

Fig. 2 Wing geometry and nodal lines of structural modes (from Ref. 6).

where

$$Q_A = A_0 + A_1 \frac{b}{v} s + A_2 \left(\frac{b}{v}\right)^2 s^2 + \sum_{j=1}^{2} \frac{B_j s}{s + (v/b)\beta_j}$$

is a model of the aerodynamic forcing terms. The matrices A_i and B_i are coefficient matrices, which are determined by a least-squares fit to numerically calculated forcing terms on the wing. To form a state space model, the aerodynamic lag states are defined as

$$x_3 \triangleq \frac{q_d B_1 s}{s + (v/b)\beta_1} \begin{bmatrix} x_1 \\ x_5 \end{bmatrix} \tag{8}$$

$$x_4 \triangleq \frac{q_d B_2 s}{s + (v/b)\beta_1} \begin{bmatrix} x_1 \\ x_5 \end{bmatrix} \tag{9}$$

The actuator is modeled by the third-order transfer function

$$\frac{\delta(s)}{\delta_c(s)} = \frac{K_A)}{(s+p)(s^2 + 2\zeta\omega_n s + \omega_n^2)}$$

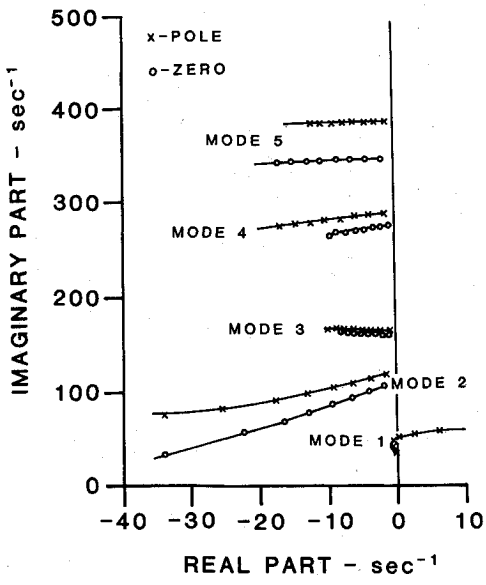

Fig. 3 Dynamic pressure root locus for uncontrolled model (inboard sensor).

where δ is the control surface deflection and δ_c is the command deflection. This can be put into the state space form

$$\dot{x}_5 = F_A x_5 + G_A \delta_c, \qquad \delta = H_A x_5 \tag{10a}$$

where δ_C is the command deflection and

$$F_A = \begin{bmatrix} 0 & 1 & 0 \\ -\omega_A^2 & -2\zeta_A\omega_A & K_A \\ 0 & 0 & -P \end{bmatrix} \quad G_A = \begin{bmatrix} 0 \\ 0 \\ 1 \end{bmatrix} \quad H_A^T = \begin{bmatrix} 1 \\ 0 \\ 0 \end{bmatrix} \tag{10b}$$

If the coefficient matrices are partitioned as

$$B_j = [B_{jF} : B_{jA}] \tag{11}$$

$$A_i = [A_{iF} : A_{iA}] \tag{12}$$

and a new set of matrices are defined as

$$\tilde{M} \triangleq M + q(b/v)^2 A_{2F} \tag{13}$$

$$\tilde{D} \triangleq D_s + q(b/v) A_{1F} \tag{14}$$

$$\tilde{K} \triangleq K_s + q A_{0F} \tag{15}$$

then a complete state space representation is

$$\begin{bmatrix} \dot{x}_1 \\ \dot{x}_2 \\ \dot{x}_3 \\ \dot{x}_4 \\ \dot{x}_5 \end{bmatrix} = \begin{bmatrix} 0 & I & 0 & 0 & 0 \\ -\tilde{M}^{-1}\tilde{K} & -\tilde{M}^{-1}\tilde{D} & -\tilde{M}^{-1} & -\tilde{M}^{-1} & T \\ 0 & q_D B_{1F} & -\frac{v}{b}\beta_1 I & 0 & q_D B_{1A} H_A F_A \\ 0 & q_D B_{2F} & 0 & -\frac{v}{b}\beta_2 I & q_D B_{2A} H_A F_A \\ 0 & 0 & 0 & 0 & F_A \end{bmatrix} \begin{bmatrix} x_1 \\ x_2 \\ x_3 \\ x_4 \\ x_5 \end{bmatrix} + \begin{bmatrix} 0 \\ 0 \\ 0 \\ 0 \\ G_A \end{bmatrix} \delta_c \tag{16}$$

$$T = -q\tilde{M}^{-1}\left[A_{0A}H_A + A_{1A}H_A F_A\left(\frac{b}{v}\right) + A_{2A}H_A F_A^2\left(\frac{b}{v}\right)^2\right] \tag{17}$$

The model used in this paper is identical to the model used in Ref. 5 except for the deletion of two gust states. In the current paper the output is taken to be the vertical wing velocity. This is calculated by using the sum of the products of the modal deflections and their respective velocity states. Velocity output can be taken at either the "inboard" or "outboard" sensor location of Fig. 2. There are 8 linear models of the wing at dynamic pressures ranging from 20-160 lb/ft^2 in increments of 20 lb/ft^2. Each model consists of 5 modes, which accounts for 10 modal states, and 10 lag states. The actuator is a third-order representation. A dynamic pressure root locus plot for the inboard sensor location is shown in Fig. 3. From this we observe that the uncontrolled system becomes unstable at a dynamic pressure of about 100 lb/ft^2 caused by an interaction between the first and second modes. While the higher modes exhibit considerable variation with dynamic pressure, the overall tendency is for increased damping in these modes.

Some Bode diagrams of the uncontrolled system with the actuator states truncated from the system are shown in Fig. 4. The inboard sensor, which is approximately at the midpoint of the control surface location, is a good approximation to the positive real model of colocated sensor and actuator and remains positive real almost until the onset of instability. With its location farther out on the wing, the outboard sensor is across the node lines of several of the higher-frequency modes. This precludes a positive real condition from being satisfied for this input/output pair. It should be noted, however, that as in any conventional control design, the additional phase lag is not serious so long as it remains well above the bandwidth of the control system. Similarly the inclusion of actuator dynamics causes all the models to lose the positive real property. See, for example, Fig. 5. So long as the region where the actuator contributes significant phase shift is outside the control bandwidth, the actuator will not adversely affect the control design.

Controller Design

In this paper we presented the results for a controller design based on a fourth-order system model using only the first two modes of the system. The design point is chosen as the case $q_D = 100$ lb/ft^2. Some results using different numbers of modes and other dynamic pressures can be found in Ref. 7. While an extensive search for the "best" design point was not carried out, these other results indicate that the current model is quite reasonable. Three different types of reduced models for both the inboard and outboard sensor locations are used. A truncation model is obtained by deleting the unmodeled states from the full model. A frequency response model is formulated by using the poles and zero associated with the first two modes of the 20th-order system. Finally, a residual mode model is obtained by assuming that the unmodeled modal states of the system take on a steady-state value. Thus, the partitioned state space equations of the first five modes

become

$$\begin{bmatrix} \dot{x}_m \\ 0 \end{bmatrix} = \begin{bmatrix} F_{11} & F_{12} \\ F_{21} & F_{22} \end{bmatrix} \begin{bmatrix} x_m \\ x_r \end{bmatrix} + \begin{bmatrix} G_1 \\ G_2 \end{bmatrix} u \qquad (18)$$

where

$x_m \sim$ model state

$x_r \sim$ residual mode states $\quad y = [H_1 : H_2] \begin{bmatrix} x_m \\ x_r \end{bmatrix}$ (19)

Solving for the model state results in

$$\dot{x}_m = [F_{11} - F_{12}F_{22}^{-1}F_{21}]x_m + [G_1 - F_{12}F_{22}^{-1}G_2]u \qquad (20)$$

$$y = [H_1 - H_2F_{22}^{-1}F_{21}]x_m + [-H_2F_{22}^{-1}G_2]u \qquad (21)$$

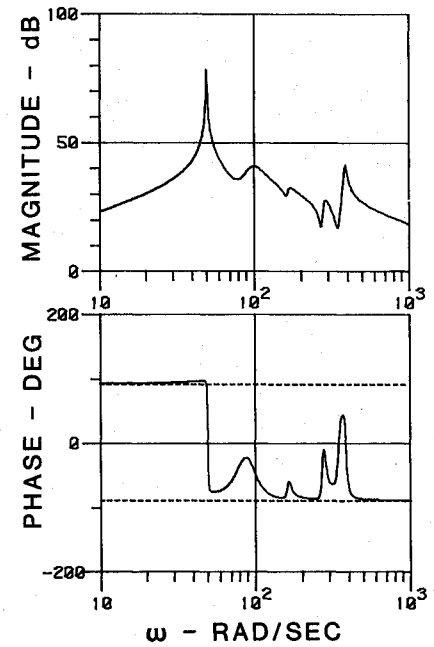

a) inboard sensor

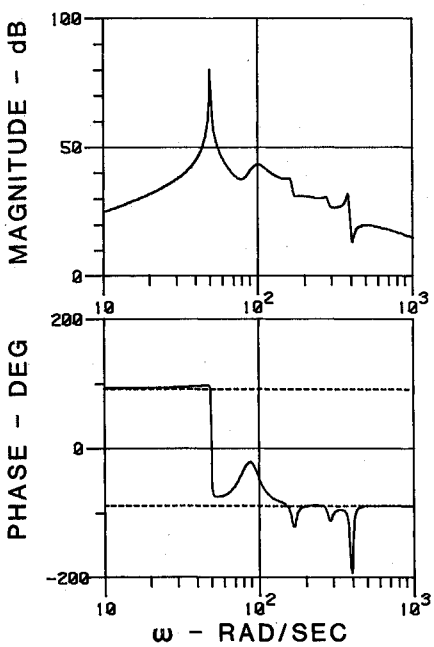

b) outboard sensor

Fig. 4 Frequency response of uncontrolled system without actuator.

So as to ensure high-frequency attenuation, this residual model was modified by dropping the term "$-H_2F_{22}^{-1}G_2u$" in Eq. (21). This coefficient was small and resulted in only a slight change in the low-frequency behavior of the mode.

The first step in the controller design is the choice of a state feedback gain matrix. For our problem this was accomplished by formulation of a model linear optimal control problem. The gain matrix is chosen to minimize the performance index

$$J = \int_0^\infty (y^TQ_Dy + u^TR_Du)\,dt \qquad (22)$$

and is solved by standard numerical means. The estimator gains are then calculated from Eqs. (5) and (6), so that the feedback transfer function is positive real. The Q matrix is chosen to have the form $Q = qI$. The choice of the value of q is based on placing the poles of $F_m - K_FH_m$ matrix sufficiently to the left of the closed-loop poles $(F_m - G_mK)$ in the s plane. Table 1 summarizes the values of Q_D, R_D, and q used for each controller. For all models the same performance index was used in the linear optimal synthesis [i.e. the same R_D, Q_D in Eqs. (22)]. To achieve the desired eigenvalue placement of the estimator, it was found that the value of "q" varied significantly between the frequency response model and the modal models. The resultant controllers are signficantly different and are summarized in Table 2. For this problem the residual and truncation models yielded essentially the same results and only the latter is explicitly discussed. Similarly, the outboard controllers are not discussed as these results differ only slightly from their inboard counterparts.

The Bode plots of the open-loop controllers are shown in Fig. 6. Note, in particular, that the truncation controller produces significant positive phase shift not present in the frequency response controller. The differences between these controllers is partly due to the crude way in which the design was formulated (using the single scalar parameter q rather than a more general form of the Q matrix). Nevertheless, in spite of these differences, both controllers do a reasonable job of controlling the divergent flutter mode as shown in the next section.

Results

The feedback controllers are first applied to the 20th-order model where the actuator states have been truncated. Recall

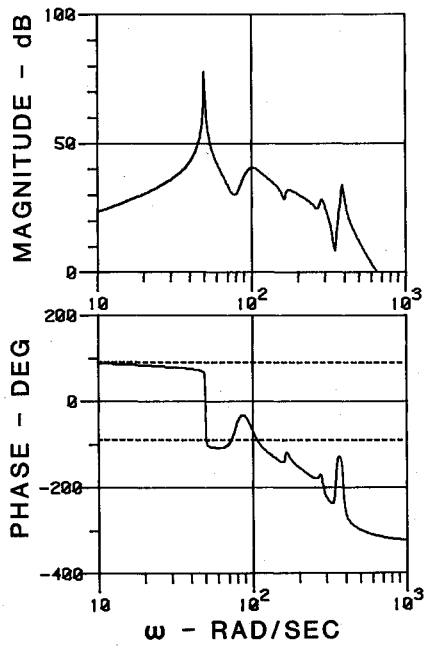

Fig. 5 Frequency response of uncontrolled system with actuator (inboard sensor).

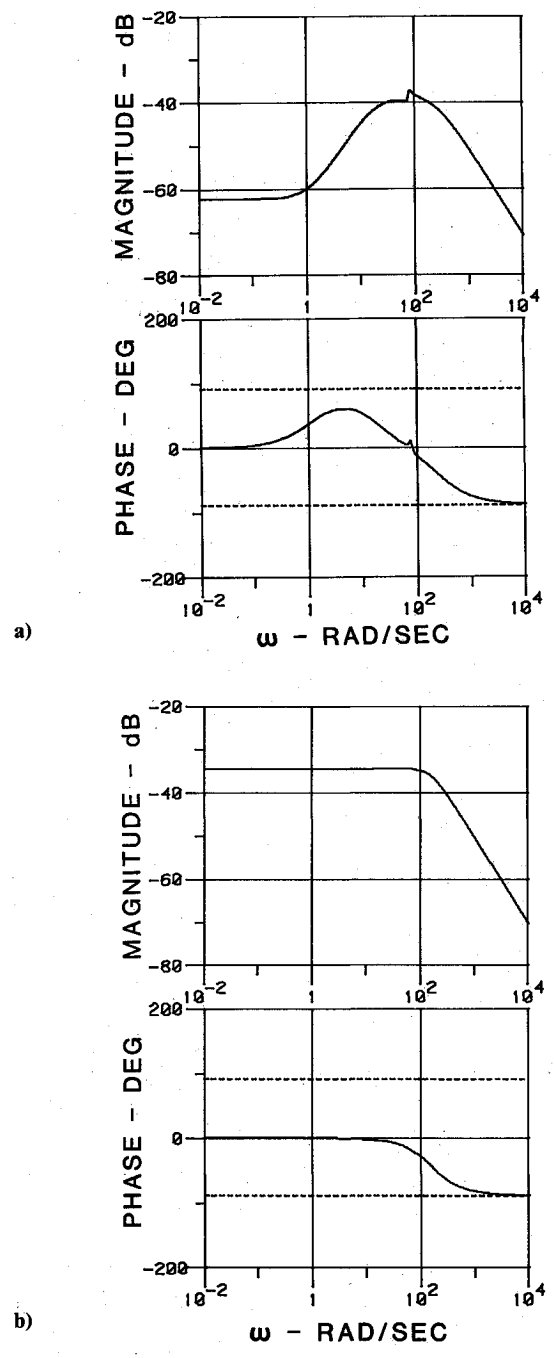

Fig. 6 Frequency response for feedback controller: a) truncation model, b) frequency response model.

Table 1 Summary of values for determining K and K_F

Model	Sensor location	Q_D	R_D	$Q=qI$
Truncation	Inboard	1	1950	0.061
Frequency response	Inboard	1	1950	3.50
Residual mode	Inboard	1	1950	0.060
Truncation	Outboard	1	3600	0.065
Frequency response	Outboard	1	3600	1.75
Residual mode	Outboard	1	3600	0.065

Table 2 Characteristics of the frequency response and residual model design models

	Model	
	Frequency response	Truncation
Model open-loop poles	$-13.3\pm95.5\,j$ $-0.2\pm49.7\,j$	$-3.63\pm87.5\,j$ $-3.4\pm53.1\,j$
Model open-loop zeros	0 $-13.0\pm78.4\,j$	0 $-3.3\pm76.0\,j$
Estimator open-loop poles	$-17.0\pm80.2\,j$ $-114\pm62.3\,j$	$-6.0\pm76.3\,j$ -227 -17.3
Estimator open-loop zeros	-104 $-16.5\pm80.8\,j$	-1.12 $-6.6\pm74.5\,j$
Model closed-loop poles (F_m-G_mk)	$-49.9\pm29.6\,j$ $-17.4\pm80.6\,j$	$-57.8\pm17.6\,j$ $-5.4\pm76.9\,j$
Estimator closed-loop poles $(F_m-K_FH_m)$	$-54.8\pm0.34\,j$ $-22.4\pm70.4\,j$	$-58.3\pm20.1\,j$ $-14.0\pm76.0\,j$

Table 3 Dynamic pressure of instability[a]

20th-order system (no actuator)		
Controller based on:	Inboard	Outboard
Truncation	150.8^1	148.6^1
Frequency response	167.3^2	165.9^2
Residual mode	151.3^1	148.8^1
23rd-order system		
Controller based on:	Inboard	Outboard
Truncation	149.8^1	147.5^1
Frequency response	145.9^2	118.6^2
Residual mode	150.4^1	147.9^1

[a]Superscript numbers indicate which mode the calculation is based on.

that, without the actuator, the system is positive real for low dynamic pressures using the inboard sensor. The outoard sensor gives a system that is never positive real. Figure 7 shows the closed-loop poles of the 20th-order system controlled by different controllers at various dynamic pressures. The same controller applied to the full system with the actuator dynamics is shown in Fig. 8. Table 3 summarizes the performance of the controllers by indicating the approximate values of the dynamic pressure of instability. Throughout this paper, modes are referred to as first mode, second estimator mode, etc. The reader is reminded that the closed-loop system has coupling between all these modes. Thus, an unstable estimator mode still results in an unstable wing vibration.

When the actuator is excluded from the full model, the controllers using the inboard sensor give a higher critical q_D than the controllers using the outboard sensor. This difference in performance is probably due to better placement of the inboard sensor, a placement resulting in a positive real system. The truncation controller and the residual mode controller appear to have very little difference in overall pole placement and thus show little difference in critical q_D. This strong similarity indicates a very weak coupling between the higher modes and the first two modes. The frequency response controller appears the most effective, giving a 67% increase in critical q_D. Using the truncation and residual mode controller results in the first mode becoming unstable as it did when uncontrolled. The frequency response controller results in the higher-frequency second estimator mode becoming unstable and an increasing damping of the first mode with increasing q_D.

As expected, the addition of the actuator dynamics degrades the overall performance of the controllers. The inboad sensor still performs marginally better than the outboard sensor. The truncation and residual mode controller show very little reduction in crucial q. Surprisingly, the frequency response model is considerably less effective than the other two controllers. The

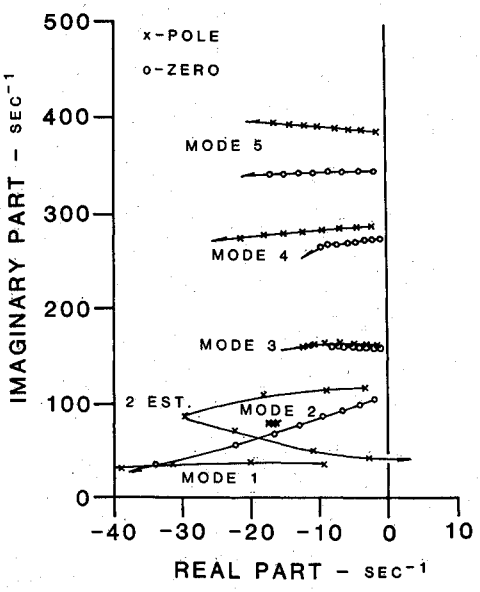

a)

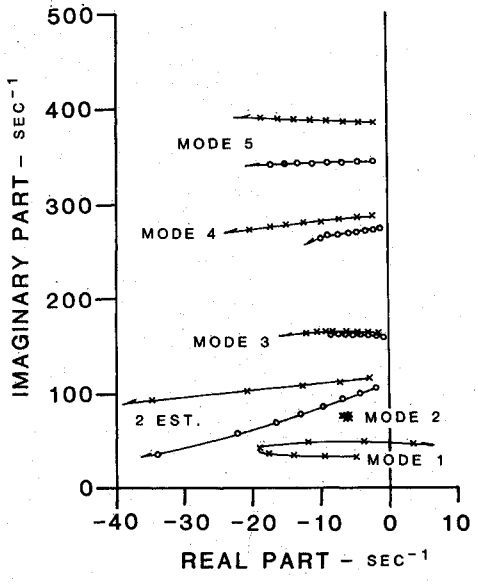

b)

Fig. 7 Closed-loop dynamic pressure root locus for 20th-order system: a) frequency response controller, b) truncation controller.

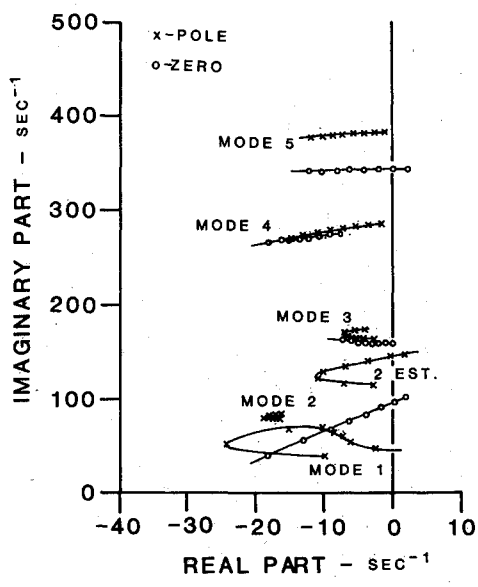

a)

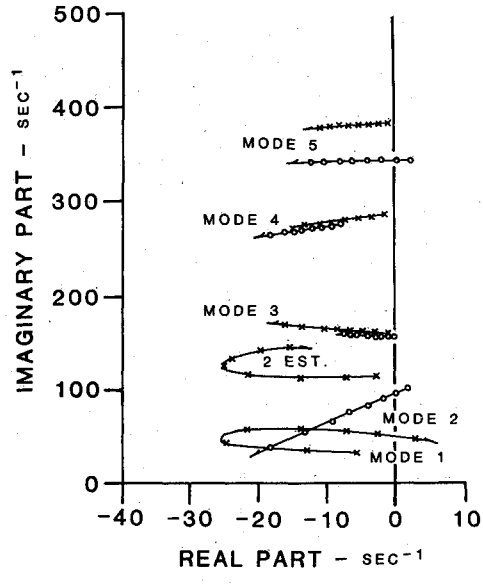

b)

Fig. 8 Closed-loop dynamic pressure root locus for 23rd-order system: a) frequency response controller, b) truncation controller.

outboard frequency response model gives only a 19% increase in dynamic pressure, far less than any other controller.

Since the actuator introduces lag at a higher frequency, it tends to affect the higher modes of the system. The inboard truncation and residual mode controllers allow both the first and second mode estimator poles to move back toward the imaginary axis. The inboard frequency response controller moves the first mode, the second mode estimator, and the third mode poles back toward the imaginary axis. The outboard truncation and residual mode controllers have an opposite behavior on the second mode estimator and third mode poles. The third mode poles come much closer to an instability than did the second mode estimator poles for the inboard sensor. The outboard frequency response controller does not have the third mode pole migration as in the inboard case, but the second mode estimator becomes unstable long before the second estimator mode of the inboard case.

The poor performance of the frequency response controller on the full model may also be explained by this same argument. The actuator is relatively fast and imposes very little phase lag in the frequency range of the first mode. The truncation controller applied to the nonactuator system results in the first mode going unstable at a given critical q_D. When the actuator is included, the primary effect is on the higher modes where the actuator has a more appreciable lag. So, the dynamic pressure of instability remains relatively unaffected whether the actuator is included or not. In contrast, the frequency response controller applied to the nonactuator system allows the second estimator poles to move close to an instability. The second estimator mode is in a higher-frequency range than the first mode, and thus, when the actuator is included, the effect on this near unstable mode is greater, resulting in a lower critical q_D.

Figure 9 shows a representative time response plot of the closed-loop system displacement and velocity at the inboard sensor at $q_D = 140$ psf. The system is being controlled by the controller based on the two mode truncation model. The initial conditions are a displacement of 0.1 ft from each mode and zero for the remaining states. The actuator deflection and deflection rate time response are also included. For a more complete discussion of these results, see Ref. 7.

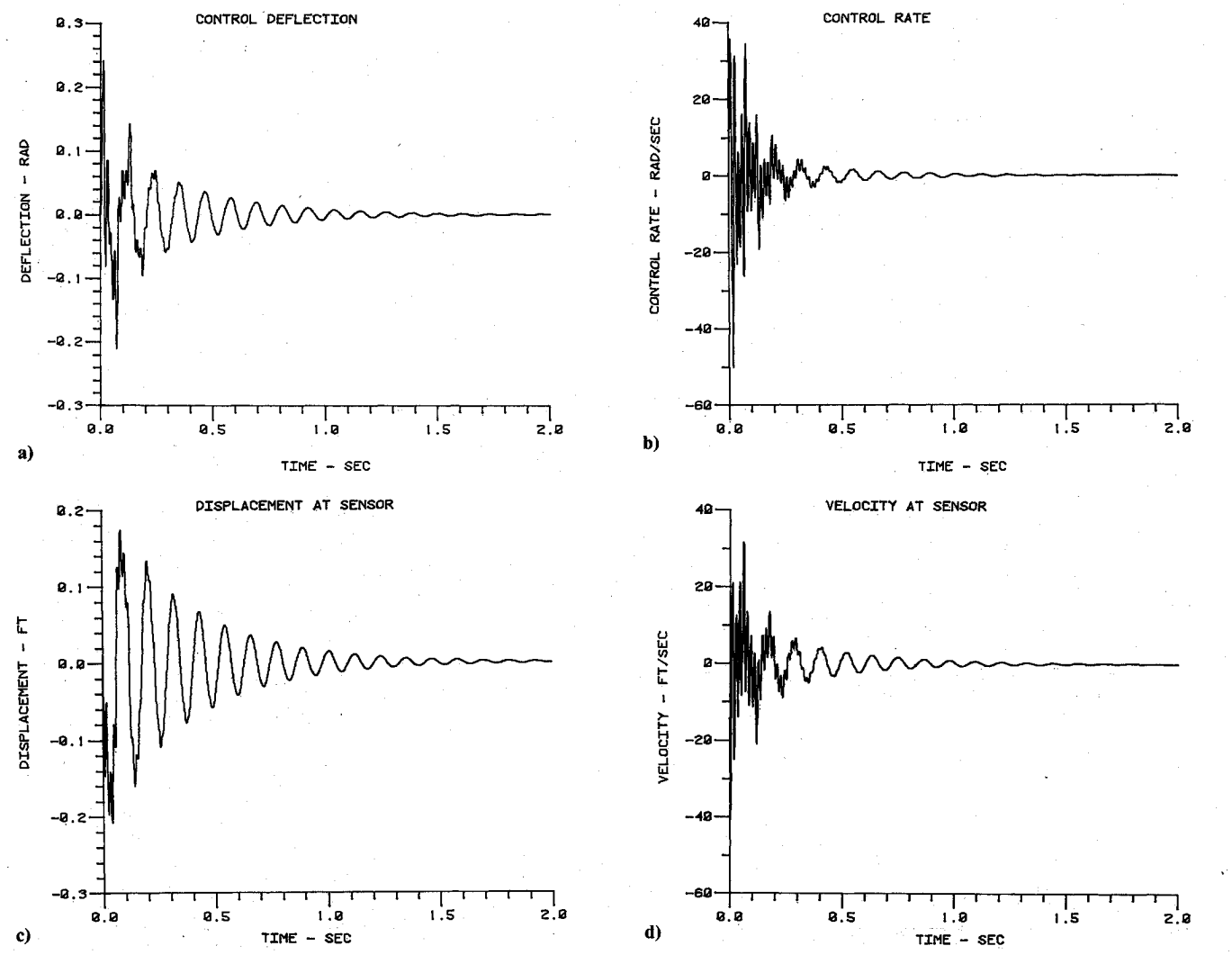

Fig. 9 Typical closed-loop time response plot; 40% above open-loop flutter dynamic pressure ($q_D = 140$ lb/ft^2): a) control deflection, b) control rate, c) displacement at sensor, d) velocity at sensor.

Conclusions

The results show that the positive real feedback methodology is a useful approach for the design of stable, robust feedback controllers. Even though positive realness is too restrictive to be universally true for the exact model, the approximation tends to be quite valid except near the flutter condition, when aerodynamic terms dominate, and at high frequencies, where actutor dynamics play a significant role in the behavior of the system. For the model problem analyzed, flutter dynamic pressure is increased by over 50%. Additional work that explicitly integrates the actuator dynamics into the control model is expected to extend this margin still further. The application of positive real feedback to the flutter control problem requires only modest computational effort while yielding a robust control design.

Acknowledgments

This work was partially supported by the Air Force under Contract AF-F33615-82-K-3609.

References

[1]Slater, G.L., "Flutter Mode Suppression Using Hyperstability Feedback," AIAA Paper 82-0368, Jan. 1982.

[2]Anderson, B.D.O., "A System Theory Criterion for Positive Real Matrices," *SIAM Journal of Control,* Vol. 5, Feb. 1967, pp. 171-182.

[3]Benhabib, R.J., Iwens, R.P., and Jackson, R.L., "Stability of Large Space Structure Control Systems Using Positivity Concepts," *Journal of Guidance and Control,* Vol. 4, Sept.-Oct. 1981.

[4]Landau, Y.D., *Adaptive Control; Model Reference Approach,* Marcel Dekker, Inc. 1979.

[5]Mukhopadhyay, V., Newson, J.R., and Abel, I., "A Method for Obtaining Reduced-Order Control Laws for High-Order Systems Using Optimization Techniques," NASA TP-1876, Aug. 1981.

[6]Newson, J.R., Abel, I., and Dunn, H.J., "Application of Two Design Method for Active Flutter Suppression and Wind-Tunnel Test Results," NASA TP1653, May 1980.

[7]Takahashi, M., "Estimator Synthesis for Flutter Control Using Positivity of Transfer Matrices," M.S. Thesis, Department of Aerospace Engineering and Applied Mechanics, University of Cincinnati, OH, Rept. ADC 84-1, 1984.